MDPI

Brief Report

Comparison of Mean Properties of Turbulent Pipe and Channel Flows at Low-to-Moderate Reynolds Numbers

Carmine Di Nucci [1],* and Rafik Absi [2]

1   Civil, Construction-Architectural and Environmental Engineering Department (DICEAA), University of L'Aquila, Piazzale Ernesto Pontieri 1, Monteluco di Roio, 67100 L'Aquila, Italy

2   ECAM-EPMI–Ecole Supérieure d'Ingénieurs en Génie Electrique, Productique et Management Industriel, LR2E-Lab, Laboratoire Quartz (EA 7393), 13 Boulevard de l'Hautil, 95092 Cergy-Pontoise, France

*   Correspondence: carmine.dinucci@univaq.it

Abstract: We focus on the fully developed turbulent flow in circular pipes and channels. We provide a comparison of the mean velocity profiles, and we compute the values of the global indicators, such as the skin friction, the mean velocity, the centerline velocity, the displacement thickness, and the momentum thickness. The comparison is done at low-to-moderate Reynolds numbers. For channel flow, we deduced the mean velocity profiles using an indirect turbulent model; for pipe flow, we extracted the needed information from a direct numerical simulation database available in the open literature. A one-to-one comparison of these values at identical Reynolds numbers provides a deep insight into the difference between pipe and channel flows. This line of reasoning allows us to highlight some deviations among the mean velocity profiles extracted from different pipe databases.

Keywords: turbulence; internal flow; mean velocity profile; skin friction; indirect turbulence model

1. Introduction

In this note, we focus on the fully developed turbulent flow of Newtonian fluids in circular pipes and very large channels, both with smooth walls, at low-to-moderate Reynolds numbers. We do not consider the compressible effects [1–9]. We provide a comparison of the Mean Velocity Profiles (MVP), and we compute the values of the global indicators, such as the skin friction, the displacement thickness, the momentum thickness, the centerline velocity, and the mean velocity. The similarities and differences in turbulent pipe and 2D channel flows (referred to as internal turbulent flows) have generated considerable research attention. Previous results show that close to the wall, in the inner layer (the viscous sublayer plus the buffer layer, see, e.g., [10]), the MVPs are essentially indistinguishable [11–14]; in the outer layer, (the log-law layer plus the wake layer [10]) the MVPs show remarkable differences [15–17].

Coles [18] provides a comprehensive study on the MVPs in the outer layer. This classical paper is about investigating and modeling deviation of data from logarithmic law. The log-wake law proposed by Coles is extended in [19,20]. Moreover, Monty [21] proposed two different formulations for the wake law for pipe and channel flows.

The key feature of turbulence is instantaneous chaotic motion. The interaction of inner and outer regions is an intrinsically nonlinear process [22]. The turbulent flow is subjected to inertial and viscous forces acting with different intensities at different wall-normal positions. The internal turbulent flows are composed of recurrent and quantifiable coherent structures, having different length scales (the Reynolds number can be viewed as a measure of separation between the largest inertial and the smallest viscous scales). The need for adequate scale separation when considering coherent structures in pipe/channel turbulent flow is given in [22]. Interactions between these coherent structures are different in pipe and channel flows [23–25]. The turbulence, which is generated at the wall, is transported outward; the different available space in the pipe/channel core region causes different

turbulence behavior. In a channel, the space for turbulence to be transported and to be developed is constant along the wall-normal coordinate; in a pipe, this space is successively reduced to zero toward the center. In a pipe, this leads to more intense interactions between turbulent structures.

DNS data [21,26] and experiment [27–29] databases allow us to elucidate the statistics on the velocity fluctuations in pipe and channel flows. The streamwise turbulence intensities in the pipe and channel flows show no significant differences in the inner and outer layers; the wall-normal and spanwise turbulence intensities in pipe flow are larger than those of channel flow in the outer layer.

In this note, we provide a comparison over a range of Re_τ from 180 to 2000, where $Re_\tau = \Theta u_\tau / v$ is the friction Reynolds number, v the kinematic viscosity, Θ the pipe radius or the channel half-height, $u_\tau = \sqrt{\tau_w/\rho}$ the friction velocity, τ_w the wall shear stress, and ρ the fluid density. For channel flows, we deduce the MVP by using the Indirect Turbulence Model (ITM) proposed in [30]; for pipe flows, we extract the needed information from the Direct Numerical Simulation (DNS) database available in the open literature [26,31,32]. A one-to-one comparison of turbulent pipe and channel flows at the identical friction Reynolds numbers allows us to define the global indicators and to investigate the Reynolds number effects. This line of reasoning allows us to observe some deviations among the MVPs extracted from the two different pipe DNS databases. After some remarks on the ITM (Section 2), in Section 3 we illustrate and discuss the results of the comparison, and we highlight the discrepancies in global parameters for pipe flows. In Section 4 we summarize the findings quantitatively, and we give the concluding comments.

2. Indirect Turbulence Model (ITM)

In this section, we re-examine the ITM as proposed in [30], which allows us to derive the MPV for 2D turbulent channel flows in smooth walls. By assuming a hyperbolic trend of the turbulent shear stress, the mean velocity u^+ in the streamwise direction is expressed as a function of the wall-normal coordinate y^+ and of the friction Reynolds number $Re_\tau = y^+{}_{max}$, where the superscript $+$ stands for normalization with the inner variable, the friction velocity u_τ, and the fluid kinematic viscosity v. According to the ITM, the relationship $u^+ = u^+(y^+, Re_\tau)$ is given as:

$$u^+ = (\varphi_1 + \psi_1/2)y^+/y^+{}_{max} + \varphi_2\left(y^+/y^+{}_{max}\right)^2 + \varphi_3\psi_3 + \varphi_3 \ln \psi_2 \tag{1}$$

where:

$$\psi_1 = \sqrt{P_1(y^+/y^+{}_{max})^2 + P_2 y^+/y^+{}_{max} + P_3} \tag{2}$$

$$\psi_2 = \left(P_2/\sqrt{P_1} + 2\sqrt{P_3}\right)/\left(\left(2P_1 y^+/y^+{}_{max} + P_2\right)/\sqrt{P_1} + 2\psi_1\right) \tag{3}$$

$$\psi_3 = \psi_1 - \sqrt{P_3} \tag{4}$$

$$\varphi_1 = Re_\tau + D \tag{5}$$

$$\varphi_2 = \left(B - y^+{}_{max}\right)/2 \tag{6}$$

$$\varphi_3 = \left(\sqrt{P_1}P_2\right)/\left(4P_1{}^{3/2}\right) \tag{7}$$

$$\varphi_4 = \left(P_2{}^2 - 4P_1 P_3\right)/\left(8P_1{}^{3/2}\right) \tag{8}$$

$$P_1 = B^2 - C \tag{9}$$

$$P_2 = 2(BD - E) \tag{10}$$

$$P_3 = D^2 + C + 2E \tag{11}$$

$$B = Re_\tau(1 - f_1) \tag{12}$$

$$C = \left(y^+{}_{max}{}^2 - By^+{}_{max}\right)/f_2 - y^+{}_{max}{}^2 + 2By^+{}_{max} \tag{13}$$

$$D = -1/y^+_{max}\left(\left(y^+_{max}{}^2 - By^+_{max}\right)/f_3 + y^+_{max}{}^2\right) \tag{14}$$

$$E = \left(y^+_{max}{}^2 - By^+_{max}\right)/f_4 + y^+_{max}{}^2 - By^+_{max} + Dy^+_{max} \tag{15}$$

$$f_1 = \left(3.655y^+_{max}{}^2 + 25,704.994y^+_{max} - 55,013.808\right)\cdot10^{-6} \tag{16}$$

$$f_2 = \left(6.991y^+_{max}{}^2 + 39,476.172y^+_{max} - 2,873,405.419\right)\cdot10^{-6} \tag{17}$$

$$f_3 = \left(-7.409y^+_{max}{}^2 - 49,231.626y^+_{max} + 556,178.423\right)\cdot10^{-6} \tag{18}$$

$$f_4 = \left(-23.766y^+_{max}{}^2 - 82,908.798y^+_{max} + 4,325,049.776\right)\cdot10^{-6} \tag{19}$$

We underline that the ITM appears as a generalization of the log-law in wall-bounded turbulent flows (in both models, the turbulent shear stress exhibits a hyperbolic trend). In comparison to the very simple structure of the log-law, the ITM provides a complex relationship $u^+ = u^+(y^+, Re_\tau)$; on the other hand, this relationship satisfies both the boundary condition at $y^+ = 0$, $u^+(y^+ = 0) = 0$, and the centerline condition at $y^+ = Re_\tau$, $\frac{d}{dy^+}u^+(y^+ = Re_\tau) = 0$ [30].

In Figure 1, we show the comparison of the MPV given by Equation (1) versus the channel DNS data [33–38] (the corresponding information is given in Table 1).
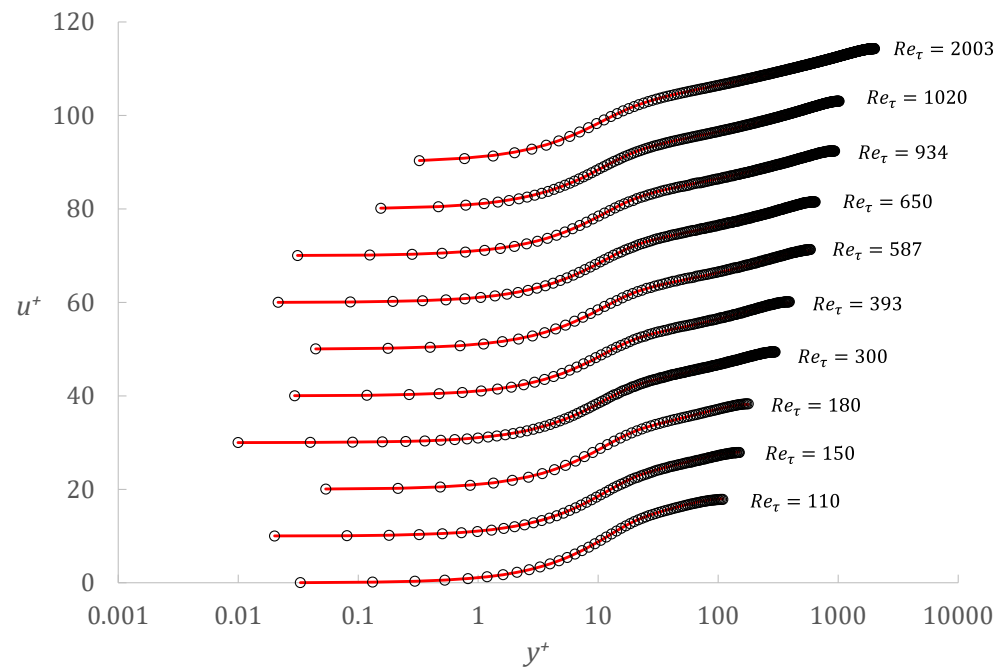

Figure 1. MVP; ○ DNS data; and − ITM. The plots are shifted vertically by 10 units.

Table 1. Re_τ, y^+_{max}, and Hellinger distance He.

Re_τ	y^+_{max}	HD
110	109.43	$1.21\cdot10^{-1}$
150	150.00	$3.20\cdot10^{-1}$
180	178.12	$1.39\cdot10^{-1}$
300	298.00	$3.66\cdot10^{-1}$
393	392.00	$2.84\cdot10^{-1}$
587	587.00	$2.61\cdot10^{-1}$
650	642.54	$2.72\cdot10^{-1}$
934	933.96	$2.83\cdot10^{-1}$
1020	1016.36	$3.93\cdot10^{-1}$
2003	2004.30	$2.37\cdot10^{-1}$

This comparison shows a very good performance of the ITM. As a metric to measure the match between the DNS data and the ITM data, we use the Hellinger distance *HD*, given as [39]:

$$HD\left(u^+{}_{DNS}\|u^+{}_{ITM}\right) = \sqrt{2\left(\sum_{y^+=0}^{Re_\tau} \left(\left(u^+{}_{DNS}(y^+)\right)^{0.5} - \left(u^+{}_{ITM}(y^+)\right)^{0.5}\right)^2\right)} \qquad (20)$$

For all cases, *HD* is very close to zero (see Table 1).

In Figures 2–6, we compare the global indicators extracted from the DNS database and from the ITM (details are given in Table 2).
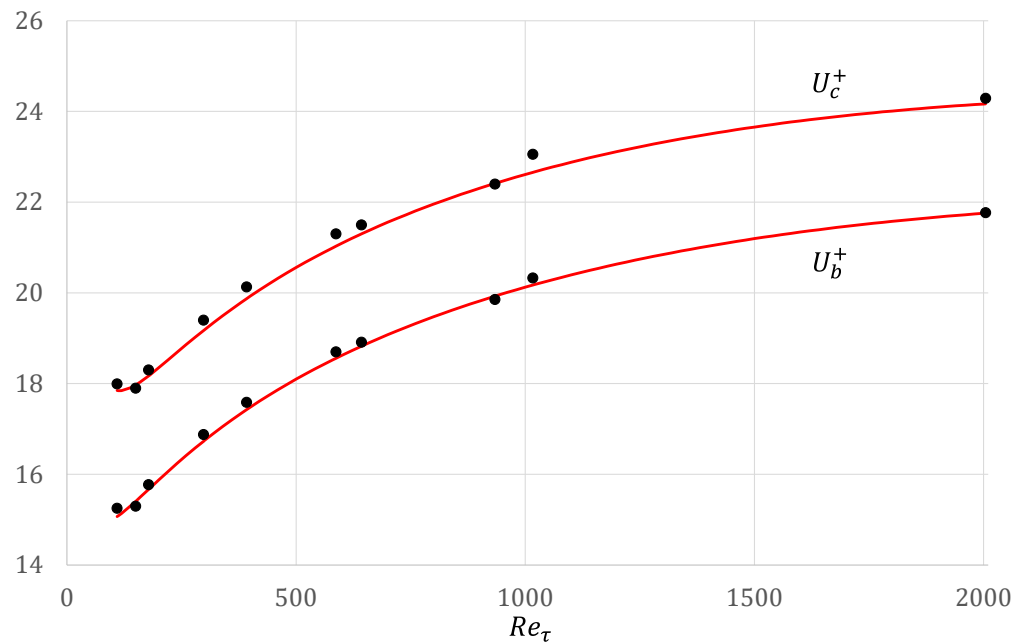

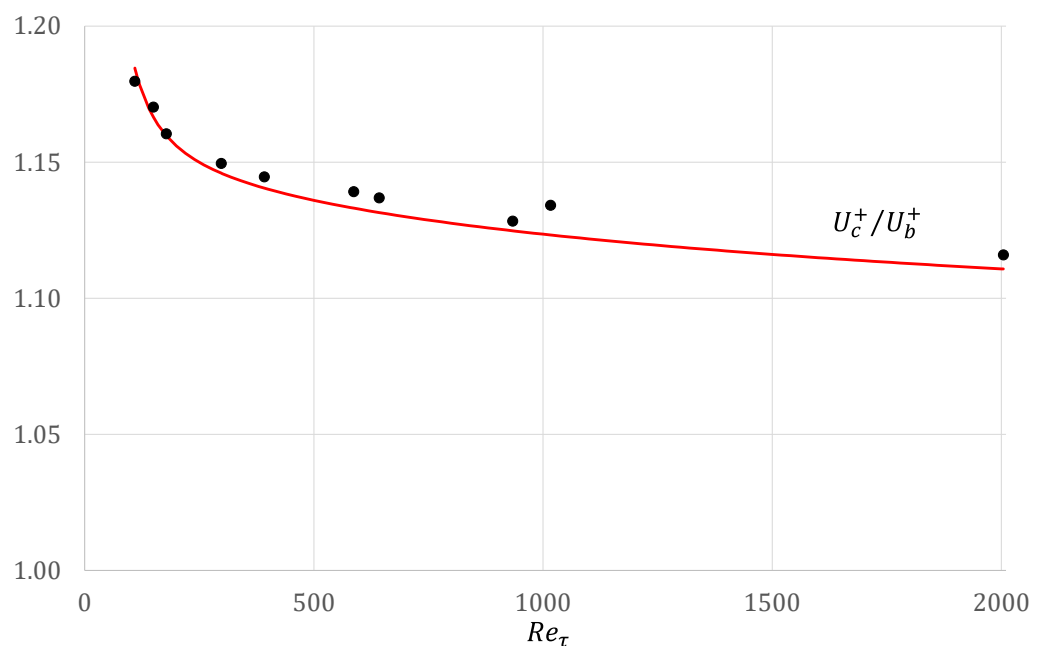**Figure 2.** Trend of the mean velocity $U_b{}^+$ and of the centerline velocity $U_c{}^+$; • DNS data; and − ITM.

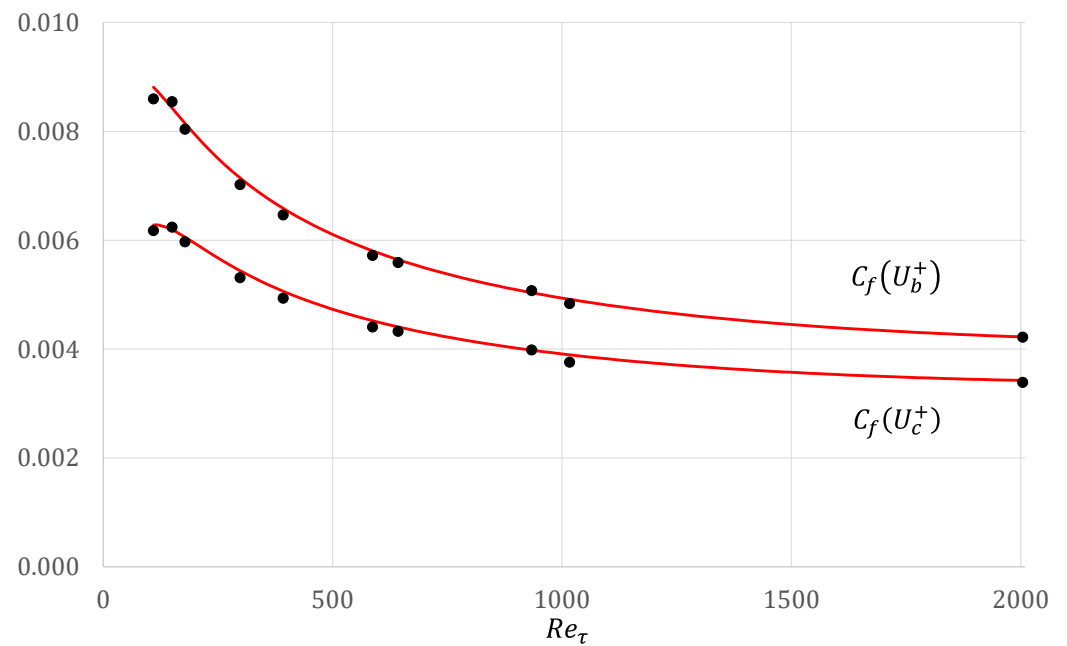**Figure 3.** Trend of the ratio $U_c{}^+/U_b{}^+$; • DNS data; and − ITM.

Figure 4. Trend of the skin friction based on the mean velocity $C_f\left(U_b{}^+\right) = 2/\left(U_b{}^+\right)^2$ and of the skin friction based on the centerline velocity $C_f\left(U_c{}^+\right) = 2/\left(U_c{}^+\right)^2$; • DNS data; and − ITM.
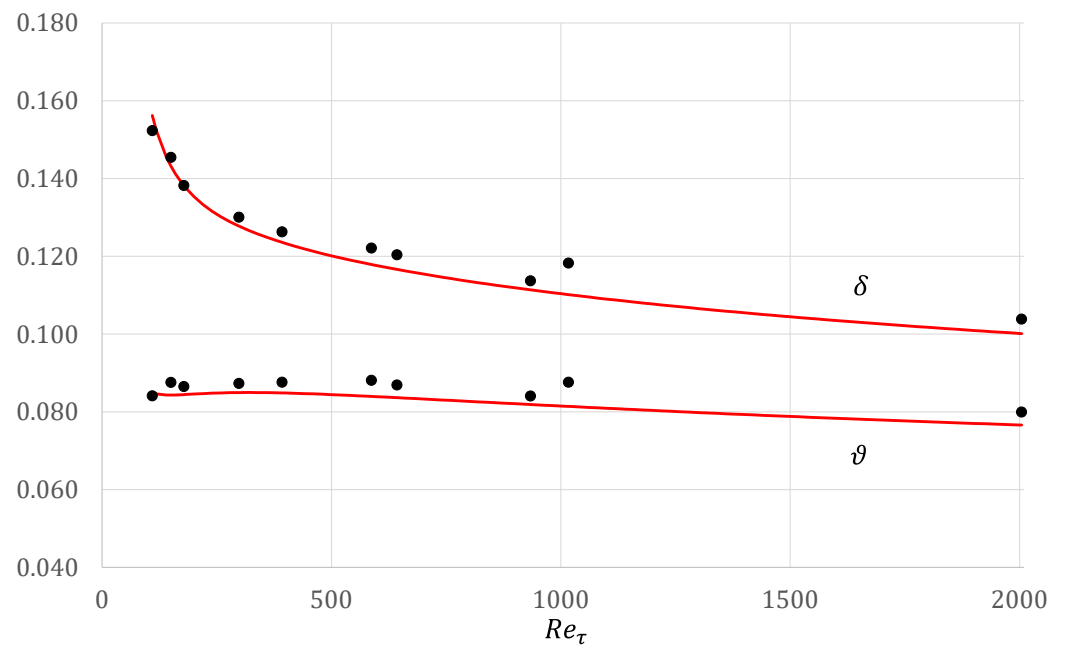
Figure 5. Trend of the displacement thickness $\delta = \int_0^1 \left(1 - \frac{u^+}{U_c{}^+}\right)\mathrm{d}\zeta$, where $\zeta = y^+/y^+{}_{max}$, and of the momentum thickness $\vartheta = \int_0^1 \frac{u^+}{U_c{}^+}\left(1 - \frac{u^+}{U_c{}^+}\right)\mathrm{d}\zeta$; • DNS data; and − ITM.
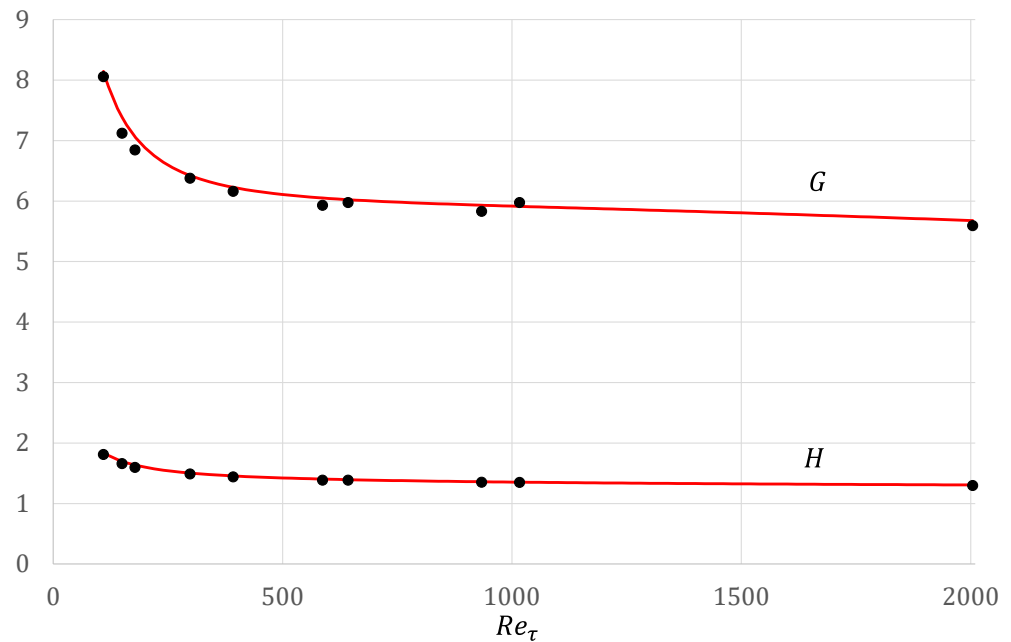
Figure 6. Trend of the first shape factor $H = \delta/\vartheta$ and of the second shape factor $G = U_c^+((H-1)/H)$; • DNS data; and — ITM.

Table 2. Mean flow properties extracted from DNS databases and from ITM. The parameters are defined as: U_b^+ is the mean velocity; U_c^+ the centerline velocity; $C_f(U_b^+)$ the skin friction based on the mean velocity $C_f(U_b^+) = 2/U_b^{+2}$; $C_f(U_c^+)$ the skin friction based on the centerline velocity $C_f(U_c^+) = 2/U_c^{+2}$; δ the displacement thickness $\delta = \int_0^1 \left(1 - \frac{u^+}{U_c^+}\right) d\zeta$, where $\zeta = y^+/y^+_{max}$; ϑ the momentum thickness $\vartheta = \int_0^1 \frac{u^+}{U_c^+}\left(1 - \frac{u^+}{U_c^+}\right)d\zeta$; H the first shape factor $H = \delta/\vartheta$; and G the second shape factor $G = U_c^+((H-1)/H)$.

Database/ Error	Re_τ	y^+_{max}	U_b^+	U_c^+	U_c^+/U_b^+	$C_f(U_b^+)$	$C_f(U_c^+)$	δ	ϑ	H	G
	110	109.43	15.25	17.99	1.18	$8.60 \cdot 10^{-3}$	$6.18 \cdot 10^{-3}$	$1.52 \cdot 10^{-1}$	$8.41 \cdot 10^{-2}$	1.81	8.06
	150	150.00	15.30	17.90	1.17	$8.55 \cdot 10^{-3}$	$6.24 \cdot 10^{-3}$	$1.45 \cdot 10^{-1}$	$8.76 \cdot 10^{-2}$	1.66	7.12
	180	178.12	15.77	18.30	1.16	$8.04 \cdot 10^{-3}$	$5.97 \cdot 10^{-3}$	$1.38 \cdot 10^{-1}$	$8.65 \cdot 10^{-1}$	1.60	6.85
	300	298.00	16.88	19.40	1.15	$7.02 \cdot 10^{-3}$	$5.31 \cdot 10^{-3}$	$1.30 \cdot 10^{-1}$	$8.73 \cdot 10^{-2}$	1.49	6.38
DNS	393	392.00	17.59	20.13	1.14	$6.47 \cdot 10^{-3}$	$4.94 \cdot 10^{-3}$	$1.26 \cdot 10^{-1}$	$8.77 \cdot 10^{-2}$	1.44	6.16
	587	587.00	18.70	21.30	1.14	$5.72 \cdot 10^{-3}$	$4.41 \cdot 10^{-3}$	$1.22 \cdot 10^{-1}$	$8.81 \cdot 10^{-2}$	1.39	5.93
	650	642.54	18.91	21.50	1.14	$5.59 \cdot 10^{-3}$	$4.33 \cdot 10^{-3}$	$1.20 \cdot 10^{-1}$	$8.69 \cdot 10^{-2}$	1.38	5.98
	934	933.96	19.85	22.40	1.13	$5.07 \cdot 10^{-3}$	$3.99 \cdot 10^{-3}$	$1.14 \cdot 10^{-1}$	$8.41 \cdot 10^{-2}$	1.35	5.83
	1020	1016.36	20.33	23.06	1.13	$4.84 \cdot 10^{-3}$	$3.76 \cdot 10^{-3}$	$1.18 \cdot 10^{-1}$	$8.76 \cdot 10^{-2}$	1.35	5.98
	2003	2004.30	21.77	24.29	1.12	$4.22 \cdot 10^{-3}$	$3.39 \cdot 10^{-3}$	$1.04 \cdot 10^{-1}$	$7.99 \cdot 10^{-2}$	1.30	5.59
	110	109.43	15.16	17.85	1.18	$8.71 \cdot 10^{-3}$	$6.28 \cdot 10^{-3}$	$1.51 \cdot 10^{-1}$	$8.33 \cdot 10^{-2}$	1.81	7.99
	150	150.00	15.46	17.97	1.16	$8.37 \cdot 10^{-3}$	$6.19 \cdot 10^{-3}$	$1.40 \cdot 10^{-1}$	$8.32 \cdot 10^{-2}$	1.68	7.27
	180	178.12	15.75	18.17	1.15	$8.07 \cdot 10^{-3}$	$6.06 \cdot 10^{-3}$	$1.33 \cdot 10^{-1}$	$8.28 \cdot 10^{-2}$	1.61	6.89
	300	298.00	16.75	19.17	1.14	$7.13 \cdot 10^{-3}$	$5.44 \cdot 10^{-3}$	$1.26 \cdot 10^{-1}$	$8.44 \cdot 10^{-2}$	1.50	6.36
ITM	393	392.00	17.46	19.87	1.14	$6.56 \cdot 10^{-3}$	$5.06 \cdot 10^{-3}$	$1.21 \cdot 10^{-1}$	$8.40 \cdot 10^{-2}$	1.45	6.13
	587	587.00	18.59	21.03	1.13	$5.79 \cdot 10^{-3}$	$4.52 \cdot 10^{-3}$	$1.16 \cdot 10^{-1}$	$8.31 \cdot 10^{-2}$	1.40	5.95
	650	642.54	18.84	21.30	1.13	$5.63 \cdot 10^{-3}$	$4.41 \cdot 10^{-3}$	$1.15 \cdot 10^{-1}$	$8.31 \cdot 10^{-2}$	1.39	5.96
	934	933.96	19.94	22.41	1.12	$5.03 \cdot 10^{-3}$	$3.98 \cdot 10^{-3}$	$1.10 \cdot 10^{-1}$	$8.13 \cdot 10^{-2}$	1.35	5.87
	1020	1016.36	20.18	22.66	1.12	$4.91 \cdot 10^{-3}$	$3.90 \cdot 10^{-3}$	$1.09 \cdot 10^{-1}$	$8.09 \cdot 10^{-2}$	1.35	5.87
	2003	2004.30	21.76	24.17	1.11	$4.22 \cdot 10^{-3}$	$3.42 \cdot 10^{-3}$	$9.94 \cdot 10^{-2}$	$7.63 \cdot 10^{-2}$	1.30	5.63

Table 2. *Cont.*

Database/ Error	Re_τ	y^+_{max}	U_b^+	U_c^+	U_c^+/U_b^+	$C_f(U_b^+)$	$C_f(U_c^+)$	δ	ϑ	H	G
			0.62%	0.80%	0.18%	1.26%	1.63%	1.01%	0.95%	0.06%	0.88%
			1.04%	0.38%	0.66%	2.06%	0.75%	3.90%	4.99%	1.15%	2.11%
			0.16%	0.73%	0.57%	0.32%	1.47%	3.56%	4.32%	0.79%	0.57%
			0.76%	1.19%	0.43%	1.54%	2.42%	2.90%	3.37%	0.49%	0.21%
relative error			0.73%	1.28%	0.55%	1.48%	2.61%	3.83%	4.18%	0.36%	0.47%
			0.58%	1.28%	0.70%	1.16%	2.60%	5.09%	5.72%	0.67%	0.43%
			0.37%	0.94%	0.57%	0.74%	1.90%	4.21%	4.46%	0.27%	0.25%
			0.46%	0.06%	0.40%	0.92%	0.12%	3.14%	3.34%	0.21%	0.67%
			0.72%	1.74%	1.03%	1.45%	3.56%	7.73%	7.72%	0.01%	1.77%
			0.02%	0.51%	0.49%	0.04%	1.03%	4.26%	4.56%	0.32%	0.56%
medium relative error			0.55%	0.89%	0.56%	1.10%	1.81%	3.96%	4.36%	0.43%	0.79%
maximum relative error			1.04%	1.74%	1.03%	2.06%	3.56%	7.73%	7.72%	1.15%	2.11%

Figure 2 shows that the ITM provides a good fit for the mean velocity U_b^+ (the percentual error is almost always less than 1%), while it underestimates the centerline velocity U_c^+ (although the maximum error is less than 2%).

Figure 3 shows that the underestimation of U_c^+ in the ITM is reflected in an underestimation of the ratio U_c^+/U_b^+ (although the percentual error is almost always less than 1%), while Figure 4 shows an acceptable fit in both $C_f(U_b^+)$ and $C_f(U_c^+)$.

Figure 5 shows that the underestimation of U_c^+ in the ITM is reflected in an underestimation in both parameters δ and ϑ, while Figure 5 shows an acceptable fit in both parameters G and H.

The ITM provides an accurate estimation for U_b^+, while the U_c^+ is almost always underestimated. As a consequence, some parameters, such as δ and ϑ, suffer from underestimation. From a general point of view, the obtained results show the reliability of the ITM to reproduce the global indicators of the turbulent channel flow.

3. Channel VS Pipe

In this section, we provide a comparison between the mean flow properties extracted from the pipe DNS database [26,31,32] and those deduced by the ITM. In Figure 7, we show the comparison of the MPVs. In Table 3, we give the corresponding information.

Table 3. Re_τ and y^+_{max}.

Database	Re_τ	y^+_{max}
	180	172.30
[26]	500	500.25
	1000	1001.92
	2000	2003.26
	180	181.89
[31,32]	500	495.26
	1000	1136.59
	2000	1977.24

In reference to the pipe DNS database [26] (Figure 7), the comparison confirms previous results which display that in the inner layer, the MVPs are essentially indistinguishable; in the outer layer, there are remarkable differences, principally in the wake layer. As stated in Section 2, the different available spaces in the pipe/channel core region causes different turbulent behavior: the space limitations in a pipe lead to more intense interactions between turbulent structures, with an increment of the streamwise mean velocity u^+. In reference to the pipe DNS database [31,32] (Figure 8), the MPVs present differences in both the inner and outer layers, and in the wake layer, these differences become important (as expected). We find other discordant results that can be attributed to a dissimilar performance of the

numerical schemes used in [26,31,32] when we compare the global indicators for pipe flow. Details are given in Table 4 and in Figures 9–17.
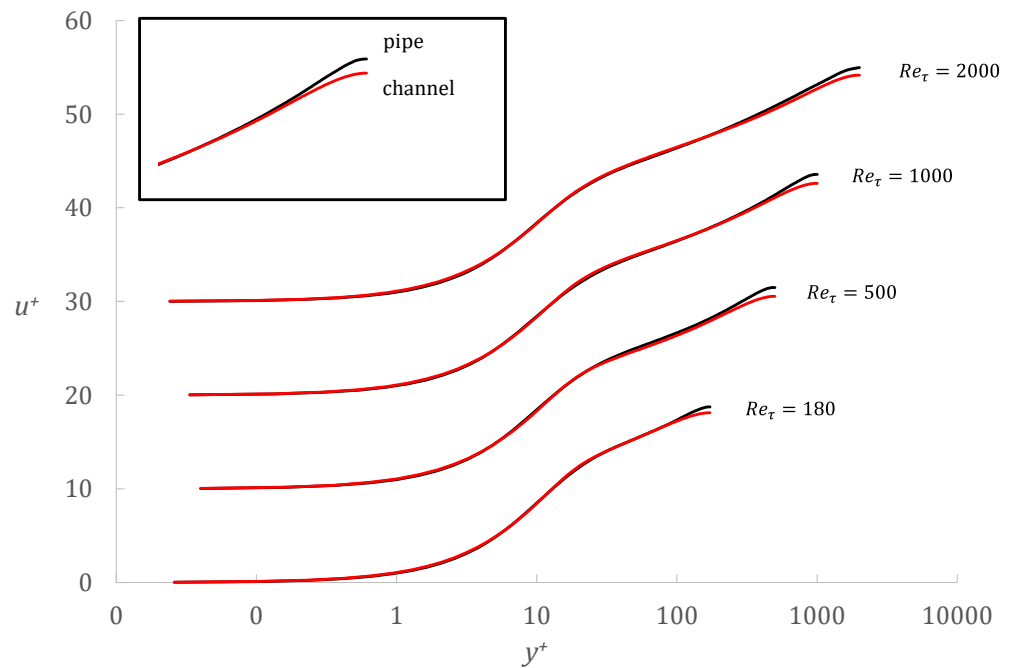

Figure 7. MVP; – pipe DNS database [26]; and – channel ITM model. The plots are shifted vertically by 10 units.
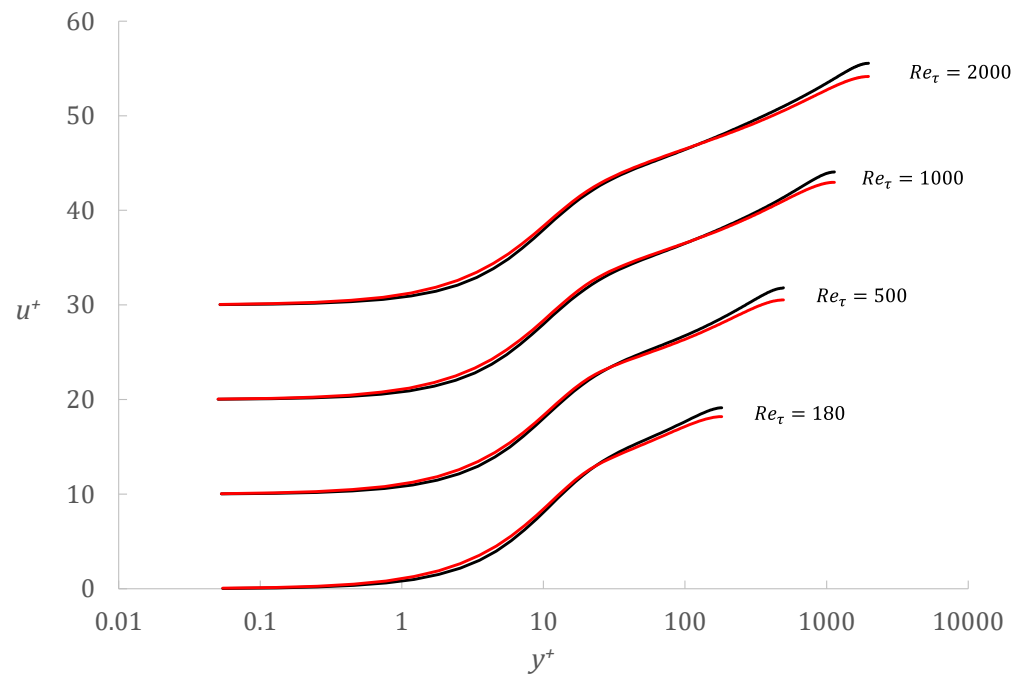

Figure 8. MVP; – DNS database [31,32]; and – channel ITM model. The plots are shifted vertically by 10 units.

Table 4. Mean flow properties extracted from pipe DNS database [26,31,32] and from channel ITM. The parameters are defined as: $U_b{}^+$ is the mean velocity; $U_c{}^+$ the centerline velocity; $C_f(U_b{}^+)$ the skin friction based on the mean velocity $C_f(U_b{}^+) = 2/U_b{}^{+2}$; $C_f(U_c{}^+)$ the skin friction based on the centerline velocity $C_f(U_c{}^+) = 2/U_c{}^{+2}$; δ the displacement thickness, which for pipe is defined as $\delta(2-\delta) = 2\int_0^1 \left(1 - \frac{u^+}{U_c{}^+}\right)(1-\zeta)\mathrm{d}\zeta$, where $\zeta = y^+/y^+{}_{max}$; ϑ the momentum thickness $\vartheta(2-\vartheta) = 2\int_0^1 \frac{u^+}{U_c{}^+}\left(1 - \frac{u^+}{U_c{}^+}\right)(1-\zeta)\mathrm{d}\zeta$; H the first shape factor $H = \delta/\vartheta$; and G the second shape factor $G = U_c{}^+((H-1)/H)$.

| Database	Re_τ	$y^+{}_{max}$	$U_b{}^+$	$U_c{}^+$	$U_c{}^+/U_b{}^+$	$C_f(U_b{}^+)$	$C_f(U_c{}^+)$	δ	ϑ	H	G
[26]	180	172.30	13.96	18.75	1.34	$1.03\cdot10^{-2}$	$5.69\cdot10^{-3}$	$2.42\cdot10^{-1}$	$1.05\cdot10^{-1}$	2.31	10.63
	500	500.25	16.87	21.50	1.27	$7.03\cdot10^{-3}$	$4.33\cdot10^{-3}$	$2.05\cdot10^{-1}$	$1.05\cdot10^{-1}$	1.95	10.50
	1000	1001.92	18.78	23.57	1.26	$5.67\cdot10^{-3}$	$3.60\cdot10^{-3}$	$1.97\cdot10^{-1}$	$1.06\cdot10^{-2}$	1.86	10.87
	2000	2003.26	20.61	24.96	1.21	$4.71\cdot10^{-3}$	$3.21\cdot10^{-3}$	$1.71\cdot10^{-1}$	$9.78\cdot10^{-2}$	1.74	10.65
[31,32]	180	181.89	14.27	19.14	1.34	$9.82\cdot10^{-3}$	$5.46\cdot10^{-3}$	$2.37\cdot10^{-1}$	$1.02\cdot10^{-1}$	2.33	10.91
	500	495.26	17.01	21.81	1.28	$6.91\cdot10^{-3}$	$4.20\cdot10^{-3}$	$2.12\cdot10^{-1}$	$1.04\cdot10^{-1}$	2.04	11.14
	1000	1136.59	19.27	24.07	1.25	$5.39\cdot10^{-3}$	$3.45\cdot10^{-3}$	$1.95\cdot10^{-1}$	$1.06\cdot10^{-1}$	1.85	11.05
	2000	1977.24	20.80	25.55	1.23	$4.62\cdot10^{-3}$	$3.06\cdot10^{-3}$	$1.83\cdot10^{-1}$	$1.03\cdot10^{-1}$	1.78	11.22
ITM	180	172.30	15.67	18.12	1.16	$8.15\cdot10^{-3}$	$6.09\cdot10^{-3}$	$1.36\cdot10^{-1}$	$8.32\cdot10^{-2}$	1.63	7.00
	180	181.89	15.79	18.20	1.15	$8.03\cdot10^{-3}$	$6.04\cdot10^{-3}$	$1.33\cdot10^{-1}$	$8.30\cdot10^{-2}$	1.60	6.81
	500	495.26	18.10	20.53	1.13	$6.10\cdot10^{-3}$	$4.75\cdot10^{-3}$	$1.18\cdot10^{-1}$	$8.38\cdot10^{-2}$	1.41	5.97
	500	500.25	18.13	20.56	1.13	$6.08\cdot10^{-3}$	$4.73\cdot10^{-3}$	$1.18\cdot10^{-1}$	$8.35\cdot10^{-2}$	1.41	6.01
	1000	1001.92	20.15	22.62	1.12	$4.93\cdot10^{-3}$	$3.91\cdot10^{-3}$	$1.09\cdot10^{-1}$	$8.09\cdot10^{-2}$	1.35	5.85
	1000	1136.59	20.50	22.97	1.12	$4.76\cdot10^{-3}$	$3.79\cdot10^{-3}$	$1.08\cdot10^{-1}$	$8.04\cdot10^{-2}$	1.34	5.80
	2000	1977.24	21.74	24.15	1.11	$4.23\cdot10^{-3}$	$3.43\cdot10^{-3}$	$9.97\cdot10^{-2}$	$7.65\cdot10^{-2}$	1.30	5.63
	2000	2003.26	21.76	24.17	1.11	$4.22\cdot10^{-3}$	$3.42\cdot10^{-3}$	$9.95\cdot10^{-2}$	$7.63\cdot10^{-2}$	1.30	5.64
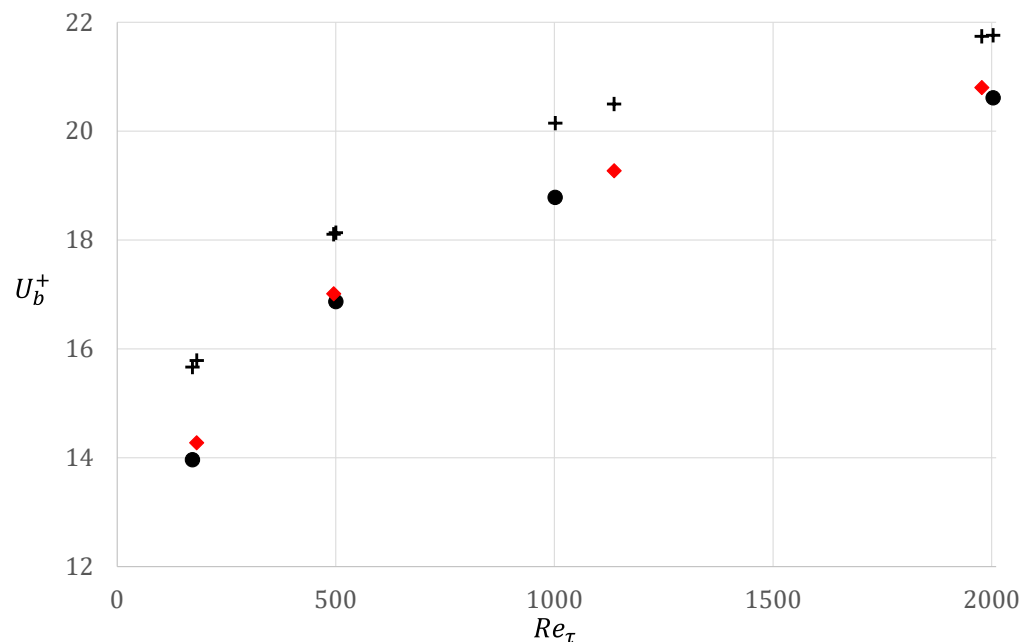
Figure 9. Trend of the mean velocity $U_b{}^+$; ● pipe DNS data [26]; ◆ pipe DNS data [31,32]; and + channel ITM.
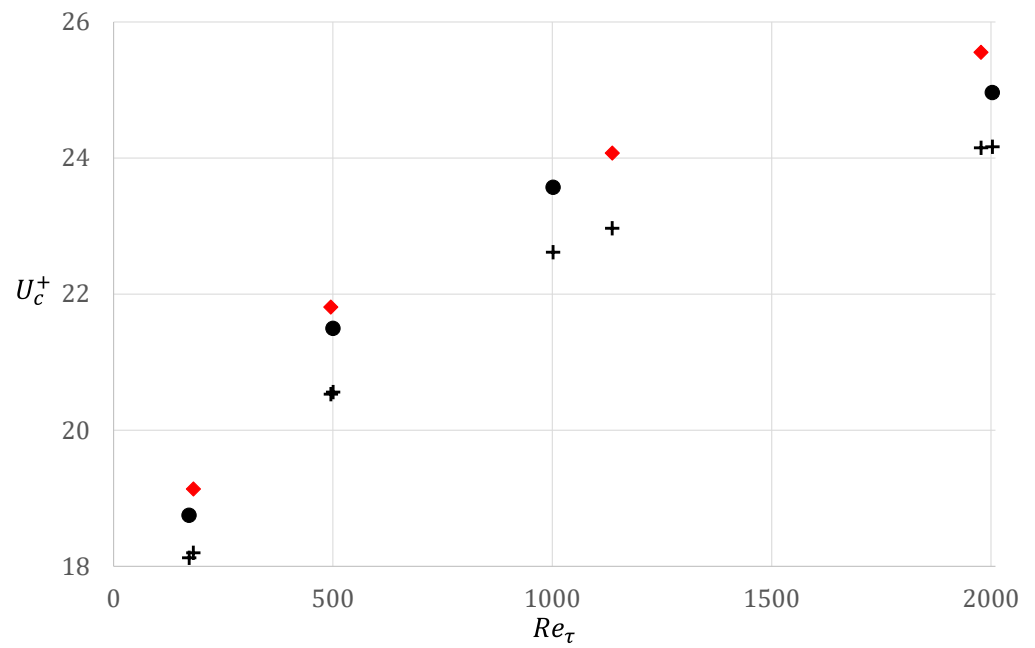
Figure 10. Trend of the centerline velocity $U_c{}^+$; ● pipe DNS data [26]; ♦ pipe DNS data [31,32]; and + channel ITM.

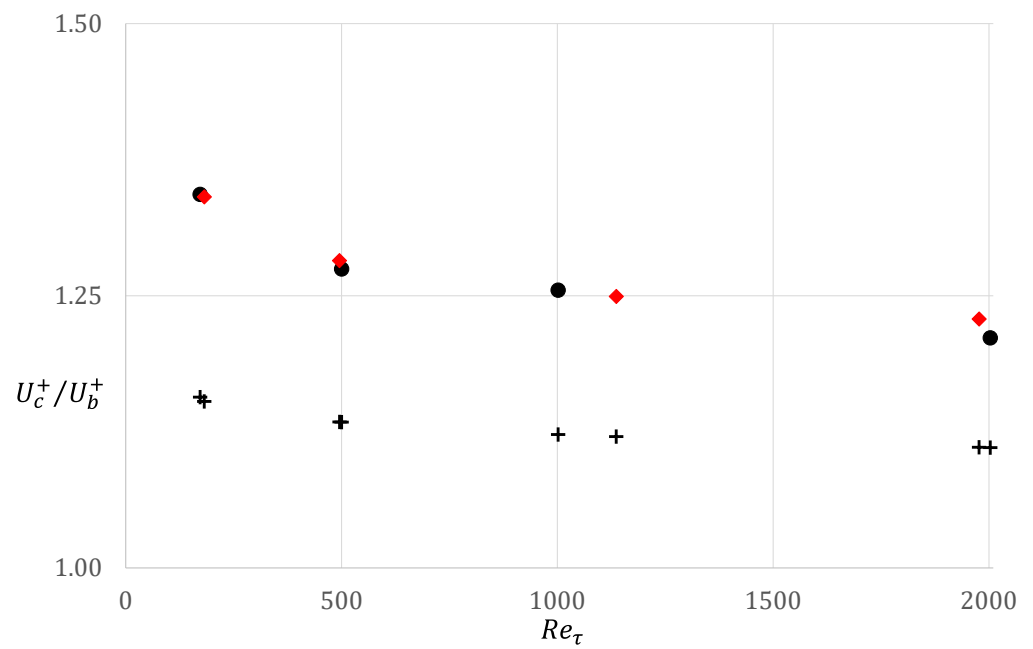**Figure 11.** Trend of the ratio $U_c{}^+/U_b{}^+$; ● pipe DNS data [26]; ♦ pipe DNS data [31,32]; and + channel ITM.
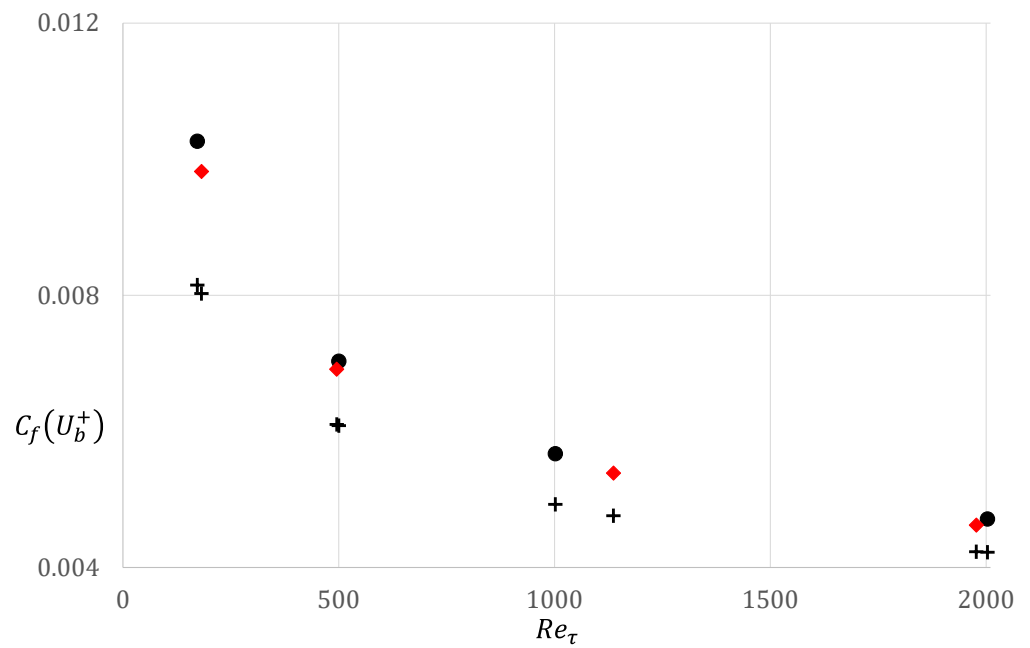
Figure 12. $C_f\left(U_b{}^+\right)$; • pipe DNS data [26]; ◆ pipe DNS data [31,32]; and + channel ITM.
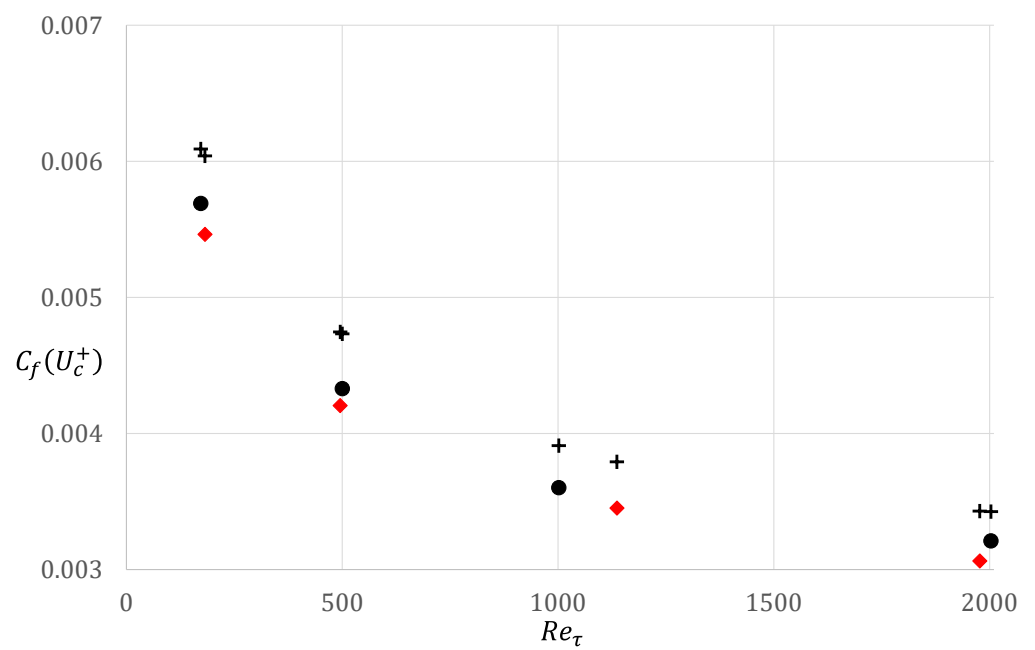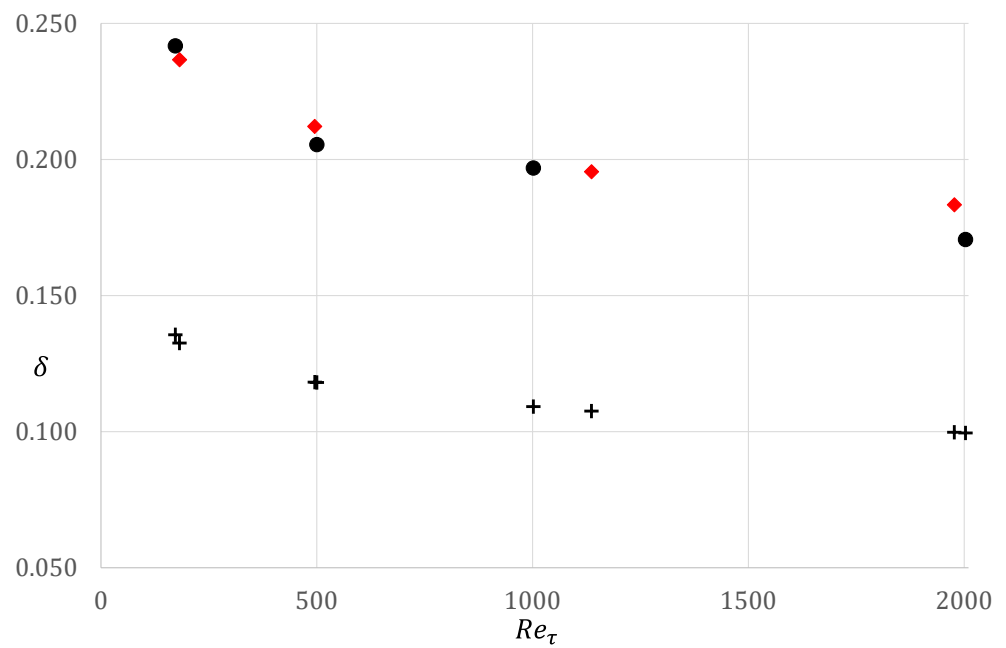

Figure 13. Trend of the skin friction $C_f\left(U_c{}^+\right)$; • pipe DNS data [26]; ◆ pipe DNS data [31,32]; and + channel ITM.

Figure 14. Trend of the displacement thickness δ; ● pipe DNS data [26]; ◆ pipe DNS data [31,32]; and + channel ITM.
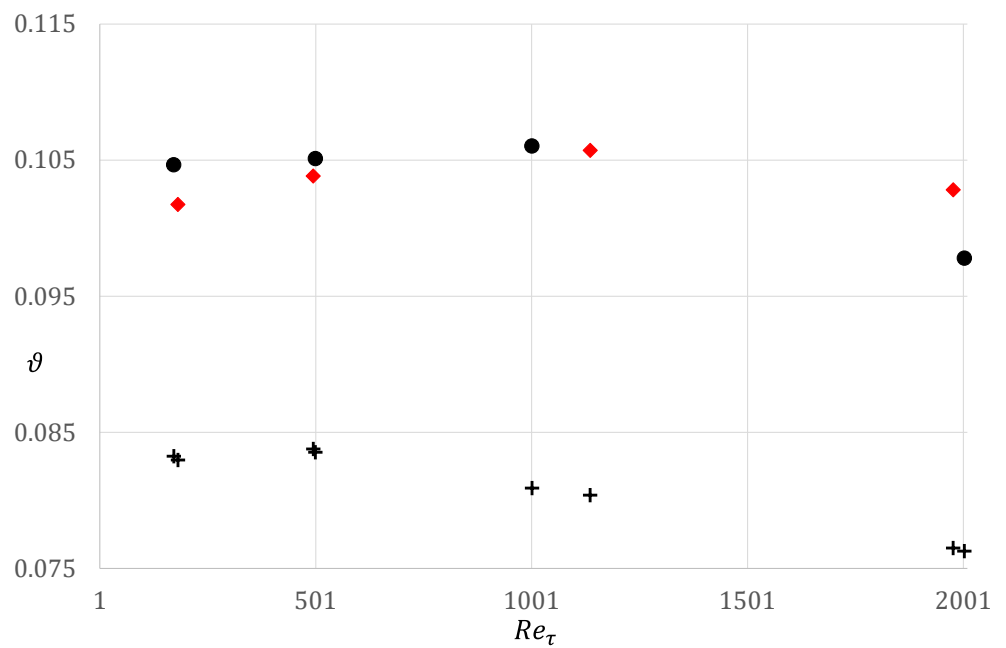
Figure 15. Trend of the momentum thickness ϑ; ● pipe DNS data [26]; ◆ pipe DNS data [31,32]; and + channel ITM.
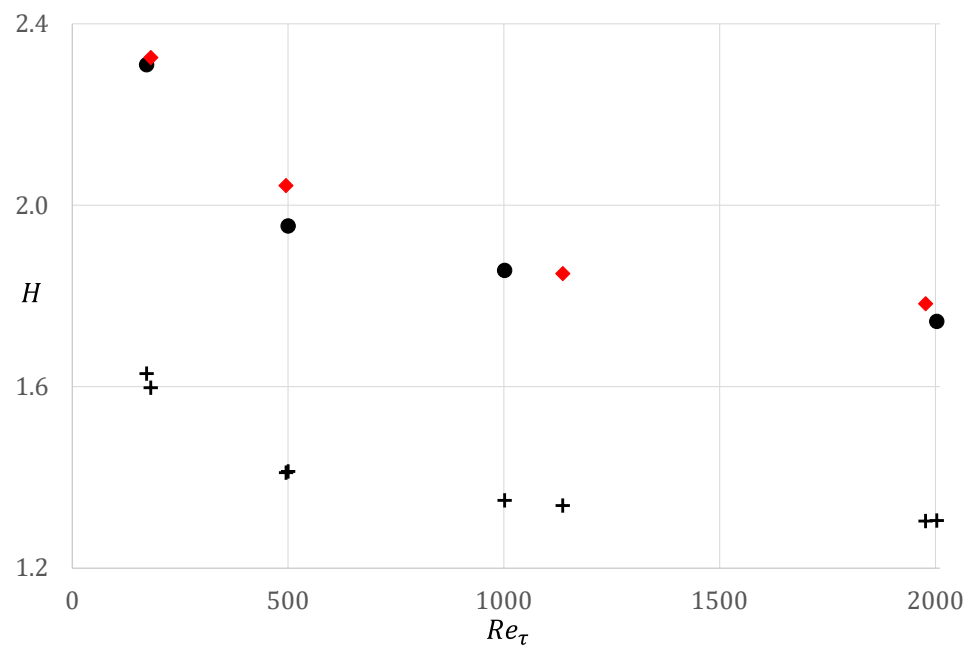
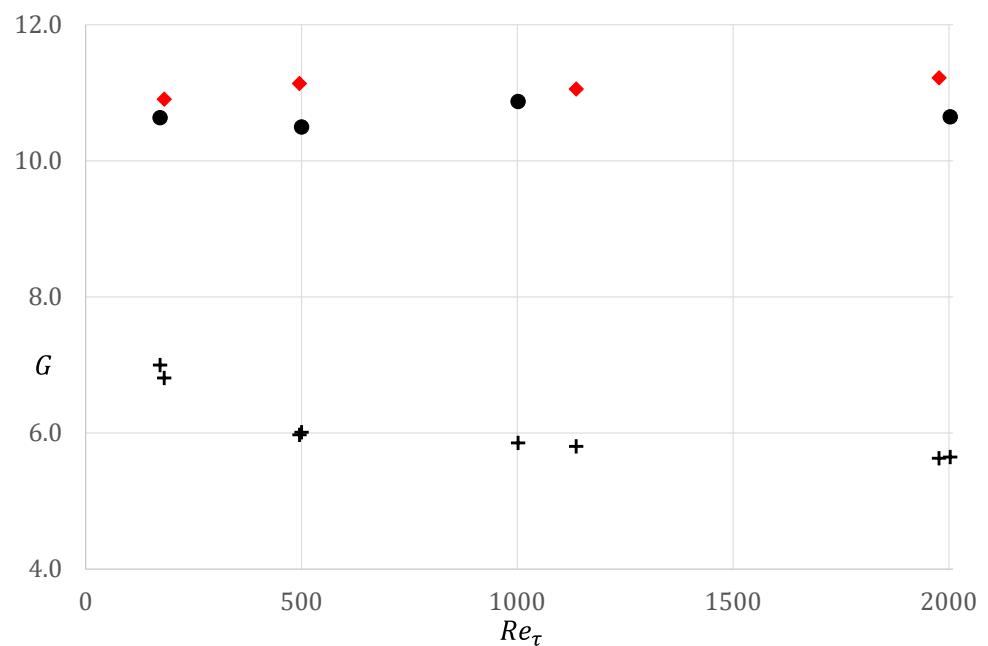**Figure 16.** Trend of the first shape factor H; • pipe DNS data [26]; ♦ pipe DNS data [31,32]; and + channel ITM.

Figure 17. Trend of the second shape factor G; • pipe DNS data [26]; ♦ pipe DNS data [31,32]; and + channel ITM.

As stated earlier, the space limitation in a pipe produces an increment in the centerline velocity U_c^+; on the other hand, due to the decrease in the cross-section area with increasing y^+, the mean velocity U_b^+ of the pipe flow is smaller than that of the channel flow.

The mean velocities U_b^+ obtained from the two different pipe DNS databases are in good agreement with each other (Figure 9); at the opposite, the centerline velocities U_c^+ extracted from the pipe DNS data [26] appear smaller than those extracted from the other pipe DNS data [31,32] (Figure 10). The other global parameters are, more or less severely, affected by these differences (Figures 11–17).

The obtained results confirm that the global indicators of pipe and channel flows are different. The mean velocity $U_b{}^+$ is larger in channel flow than in pipe flow, which determines $C_f(U_b{}^+)$ to be smaller; on the other hand, the centerline velocity $U_c{}^+$ is smaller in channel flow than in pipe flow, which causes $C_f(U_c{}^+)$ to be larger. The ratio $U_c{}^+/U_b{}^+$ for pipe flow exceeds the values in the channel flow; similar trends can be observed for the mean flow properties δ, ϑ, H, and G.

On the other hand, our results allow us to observe deviations in MVP obtained from the pipe DNS database [26,31,32]. These differences are reflected in global parameters: the mean velocity $U_b{}^+$ and the centerline velocity $U_c{}^+$ in [26] are smaller than in [31,32]; as a consequence, the respective skin frictions in [26] are larger than in [31,32]. Different trends also concern the parameters δ, ϑ, H, and G. For an accurate comparison, ideally, the datasets should consist of very similar Reynolds numbers and numerical parameters (i.e., temporal/spatial resolutions).

Finally, we notice that the data/curves in Figures 3–6, 9–14 and 16 seem to present an asymptotic behavior for $Re_\tau > 2000$ which could be related to the asymptotic behavior shown for the two coefficients of the eddy viscosity analytical model [40]. For large values of $Re_\tau > 2000$, the two coefficients of the analytical model reach asymptotic values equal, respectively, to $C_\alpha = 0.477$ and $C_1 = 2.17$. This will require further investigations in our future work.

4. Findings and Conclusions

In this brief note, we investigated the mean velocity properties of turbulent pipe and channel flows at low-to-moderate Reynolds numbers. We provided a one-to-one comparison at identical Reynolds numbers: for pipe flows, we extracted the needed information from DNS databases available in the open literature [26,31,32]; for channel flows, we used the ITM proposed in [30]. After some remarks on the ITM and on the reliability of this model to reproduce the global indicator, we examined the differences between fully developed flows in pipes and channels.

Preliminarily, we observed some deviations between the MVPs obtained from the pipe DNS databases [26,31,32]. These differences are reflected on global parameters: the mean velocity $U_b{}^+$ in [26] is about 1.5% smaller than in [31,32]; the centerline velocity $U_c{}^+$ in [26] is about 2% smaller than in [31,32]; the skin friction based on the mean velocity in [26] is about 3% larger than in [31,32]; and the skin friction based on the centerline velocity in [26] is about 4% larger than in [31,32]. These discrepancies, which can be due to a dissimilar performance of the numerical schemes used in [26,31,32], should lead to a reconsideration of the fidelity of the DNS data.

The comparison between pipe and channel flows can be summarized as follows: the mean velocity $U_b{}^+$ in channel flow is between 5% and 12% greater than in pipe flow (the larger the difference, the lower Re_τ), whereas the centerline velocity $U_c{}^+$ is about 4% smaller. The ratio $U_c{}^+/U_b{}^+$ in pipe flow is between 8% and 14% greater than in channel flow (the larger the difference, the lower Re_τ). The skin friction based on the mean velocity in pipe flow is between 8% and 21% larger than in channel flow (the larger the difference, the lower Re_τ), whereas the skin friction based on the centerline velocity is about 10% smaller. The displacement thickness in pipe flow is about 45% larger than in channel flow; the momentum thickness is between 18% and 26% larger (the larger the difference, the higher Re_τ).

References

1. Coleman, G.; Kim, J.; Moser, R. A numerical study of turbulent supersonic isothermal-wall channel flow. *J. Fluid Mech.* **1995**, *305*, 159–183. [CrossRef]
2. Huang, P.; Coleman, G.; Bradshaw, P. Compressible turbulent channel flows: DNS results and modeling. *J. Fluid Mech.* **1995**, *305*, 185–218. [CrossRef]
3. Foysi, H.; Sarkar, S.; Friedrich, R. Compressibility effects and turbulence scalings in supersonic channel flow. *J. Fluid Mech.* **2004**, *509*, 207–216. [CrossRef]
4. Ghosh, S.; Foysi, H.; Friedrich, R. Compressible turbulent channel and pipe flow: Similarities and differences. *J. Fluid Mech.* **2010**, *648*, 155–181. [CrossRef]
5. Li, X.-L.; Fu, D.-X.; Ma, Y.-W.; Liang, X. Direct numerical simulation of compressible turbulent flows. *Acta Mech. Sin.* **2010**, *26*, 795–806. [CrossRef]
6. Zhang, Y.-S.; Bi, W.-T.; Hussain, F.; Li, X.-L.; She, Z.-S. Mach-number-invariant mean-velocity profile of compressible turbulent boundary layers. *Phys. Rev. Lett.* **2012**, *109*, 054502. [CrossRef]
7. Modesti, D.; Pirozzoli, S. Reynolds and Mach number effects in compressible turbulent channel flow. *Int. J. Heat Fluid Flow* **2016**, *59*, 33–49. [CrossRef]
8. Di Nucci, C.; Pasquali, D.; Celli, D.; Pasculli, A.; Fischione, P.; di Risio, M. Turbulent bulk viscosity. *Eur. J. Mech. B Fluids* **2020**, *84*, 446–454. [CrossRef]
9. Di Nucci, C.; Celli, D.; Pasquali, D.; di Risio, M. New Dimensionless Number for the Transition from Viscous to Turbulent Flow. *Fluids* **2022**, *7*, 202. [CrossRef]
10. Heinz, S. On mean flow universality of turbulent wall flows. I. High Reynolds number flow analysis. *J. Turbul.* **2019**, *19*, 929–958. [CrossRef]
11. Absi, R.; di Nucci, C. On the accuracy of analytical methods for turbulent flows near smooth walls. *C. R. Mec.* **2012**, *340*, 641–645. [CrossRef]
12. Di Nucci, C.; Fiorucci, F. Mean velocity profiles of fully-developed turbulent flows near smooth walls. *C. R. Mec.* **2011**, *339*, 388–395. [CrossRef]
13. Absi, R. Eddy Viscosity and Velocity Profiles in Fully-Developed Turbulent Channel Flows. *Fluid Dyn.* **2019**, *54*, 137–147. [CrossRef]
14. Smits, A.J.; Hultmark, M.; Lee, M.; Pirozzoli, S.; Wu, X. Reynolds stress scaling in the near-wall region of wall-bounded flows. *J. Fluid Mech.* **2021**, *926*, A31. [CrossRef]
15. Patel, V.C.; Head, M.R. Some observations on skin friction and velocity profiles in fully developed pipe and channel flows. *J. Fluid Mech.* **1969**, *38*, 181–201. [CrossRef]
16. Huffman, G.D.; Bradshaw, P. A note on von Karman's constant in low Reynolds number turbulent flows. *J. Fluid Mech.* **1972**, *53*, 45–60. [CrossRef]
17. Eggels, J.G.; Unger, F.; Weiss, M.H.; Westerweel, J.; Adrian, R.J.; Friedrich, R.; Nieuwstadt, F.T. Fully developed turbulent pipe flow: A comparison between direct numerical simulation and experiment. *J. Fluid Mech.* **1994**, *268*, 175–210. [CrossRef]
18. Coles, D. The law of the wake in the turbulent boundary layer. *J. Fluid Mech.* **1956**, *1*, 191–226. [CrossRef]
19. Guo, J.; Julien, P.Y. Modified log-wake law for turbulent flow in smooth pipes. *J. Hydr. Res.* **2003**, *41*, 493–501. [CrossRef]
20. Guo, J. Eddy viscosity and complete log-law for turbulent pipe flow at high Reynolds numbers. *J. Hydr. Res.* **2017**, *55*, 27–39. [CrossRef]
21. Monty, J.P.; Hutchins, N.; Ng, H.C.H.; Marusic, I.; Chong, M.S. A comparison of turbulent pipe, channel and boundary layer flows. *J. Fluid Mech.* **2009**, *632*, 431–442. [CrossRef]
22. Hutchins, N.; Marusic, I. Large-scale influences in near-wall turbulence. *Philos. Trans. R. Soc. Lond. A* **2007**, *365*, 647–664. [CrossRef] [PubMed]
23. Jiménez, J. Turbulent flows over rough walls. *Annu. Rev. Fluid Mech.* **2004**, *36*, 173–196. [CrossRef]
24. Monty, J.P.; Stewart, J.A.; Williams, R.C.; Chong, M.S. Large-scale features in turbulent pipe and channel flows. *J. Fluid Mech.* **2007**, *589*, 147–156. [CrossRef]
25. Lee, J.; Ahn, J.; Sung, H.J. Comparison of large-and very-large-scale motions in turbulent pipe and channel flows. *Phys. Fluids* **2015**, *27*, 025101. [CrossRef]
26. Chin, C.; Monty, J.P.; Ooi, A. Reynolds number effects in DNS of pipe flow and comparison with channels and boundary layers. *Int. J. Heat Fluid Flow* **2014**, *45*, 33–40. [CrossRef]
27. Ng, H.C.H.; Monty, J.P.; Hutchins, N.; Chong, M.S.; Marusic, I. Comparison of turbulent channel and pipe flows with varying Reynolds number. *Exp. Fluids* **2011**, *51*, 1261–1281. [CrossRef]
28. Monty, J.P.; Chong, M.S. Turbulent channel flow: Comparison of streamwise velocity data from experiments and direct numerical simulation. *J. Fluid Mech.* **2009**, *633*, 461–474. [CrossRef]

29. Buschmann, M.H.; Indinger, T.; Gad-el-Hak, M. Near-wall behavior of turbulent wall-bounded flows. *Int. J. Heat Fluid Flow* **2009**, *30*, 993–1006. [CrossRef]

30. Di Nucci, C.; Russo Spena, A. Mean velocity profiles of two-dimensional fully developed turbulent flows. *C. R. Mec.* **2012**, *340*, 629–640. [CrossRef]

31. Pirozzoli, S.; Romero, J.; Fatica, M.; Verzicco, R.; Orlandi, P. Reynolds number trends in turbulent pipe flow: A DNS perspective. *arXiv* **2021**, arXiv:2103.13383.

32. Pirozzoli, S.; Romero, J.; Fatica, M.; Verzicco, R.; Orlandi, P. One-point statistics for turbulent pipe flow up to $Re_\tau \approx 6000$. *J. Fluid Mech.* **2021**, *926*, A28. [CrossRef]

33. Iwamoto, K.; Suzuki, Y.; Kasagi, N. Reynolds number effect on wall turbulence: Toward effective feedback control. *Int. J. Heat Fluid Flow* **2002**, *23*, 678–689. [CrossRef]

34. Iwamoto, K. *Database of Fully Developed Channel Flow*; THTLAB Internal Report No. ILR-0201; Department of Mechanical Engineering, University of Tokyo: Tokyo, Japan, 2002.

35. Abe, H.; Kawamura, H.; Matsuo, Y. Surface heat-flux fluctuations in a turbulent channel flow up to Re_τ = 1020 with Pr = 0.0025 and 0.71. *Int. J. Heat Fluid Flow* **2004**, *25*, 404–419. [CrossRef]

36. Moser, R.D.; Kim, J.; Mansour, N.N. Direct numerical simulation of turbulent channel flow up to Re_τ=1020. *Phys. Fluids* **1999**, *11*, 943–945. [CrossRef]

37. Del Álamo, J.C.; Jiménez, J.; Zandonade, P.; Moser, R.D. Scaling of the energy spectra of turbulent channels. *J. Fluid Mech.* **2004**, *500*, 135–144. [CrossRef]

38. Hoyas, S.; Jiménez, J. Scaling of the velocity fluctuations in turbulent channels up to Re_τ = 2003. *Phys. Fluids* **2006**, *18*, 011702. [CrossRef]

39. Deza, M.M.; Deza, E. *Distances and Similarities in Data Analysis*; Springer: Berlin/Heidelberg, Germany, 2013.

40. Absi, R. Reinvestigating the parabolic-shaped eddy viscosity profile for free surface flows. *Hydrology* **2021**, *8*, 126. [CrossRef]